# Long-Term Non Anesthetic Preclinical Study Available Extra-Cranial Brain Activator (ECBA) System for the Future Minimally Invasive Human Neuro Modulation

Hyungwoo Lee, *Member, IEEE*, Jun Seung Mun, Woo Ram Jung, Seunghun Lee, Joonseong Kang, Wonok Kang, Sehyeon Kim, Sung-Min Park, Duk L. Na, Young-Min Shon, and Sang Joon Kim, *Member, IEEE*

***Abstract*—In recent years, electroceuticals have been spotlighted as an emerging treatment for various severe chronic brain diseases, owing to their intrinsic advantage of electrical interaction with the brain, which is the most electrically active organ. However, the majority of research has verified only the short-term efficacy through acute studies in laboratory tests owing to the lack of a reliable miniaturized platform for long-term animal studies. The construction of a sufficient integrated system for such a platform is extremely difficult because it requires multi-disciplinary work using state-of-the-art technologies in a wide range of fields. In this study, we propose a complete system of an implantable platform for long-term preclinical brain studies. Our proposed system, the extra-cranial brain activator (ECBA), consists of a titanium-packaged implantable module and a helmet-type base station that powers the module wirelessly. The ECBA can also be controlled by a remote handheld device. Using the ECBA, we performed a long-term non-anesthetic study with multiple canine subjects, and the resulting PET-CT scans demonstrated remarkable enhancement in brain activity relating to memory and sensory skills. Furthermore, the histological analysis and high-temperature aging test confirmed the reliability of the system for up to 31 months. Hence, the proposed ECBA system is expected to lead a new paradigm of human neuromodulation studies in the near future.**

***Index Terms*—Aging test, brain activation system, biocompatible, high frequency stimulation, histologic analysis, long-term non-anesthetic preclinical study, neuro-modulation.**

Manuscript received August 1, 2020; revised September 21, 2020; accepted October 15, 2020. Date of publication October 28, 2020; date of current version December 30, 2020. (*Hyungwoo Lee and Jun Seung Moon contributed equally to this work*) (*Corresponding authors: Hyungwoo Lee; Sang Joon Kim.)*

Hyungwoo Lee, Joonseong Kang, and Sang Joon Kim are with the Samsung Advanced Institute of Technology (SAIT), Suwon 16678, South Korea (e-mail: hwlee010@gmail.com; js2k.kang@samsung.com; sangjoon0919.kim@samsung.com).

Jun Seung Mun, Wonok Kang, Sehyeon Kim, and Sung-Min Park are with the Pohang University of Science and Technology (POSTECH), Pohang 37673, South Korea (e-mail: answnstmd994@postech.ac.kr; wonokkang@postech.ac.kr; sehyeonkim@postech.ac.kr; sungminpark@postech.ac.kr).

Woo Ram Jung, Seunghun Lee, Duk L. Na, and Young-Min Shon are with the Samsung Medical Center, Seoul 06351, South Korea (e-mail: skmac@naver.com; shben.lee@samsung.com; dl1018.na@samsung.com; sonogung@gmail.com).

Color versions of one or more of the figures in this article are available online at https://ieeexplore.ieee.org.

Digital Object Identifier 10.1109/TBCAS.2020.3034444

## I. Introduction

ELECTROCEUTICALS have been accepted as one of the most distinct approaches for treating various chronic brain diseases [1]–[5]. As the brain consists of a tremendous number of electrically active components, namely active neurons and their synaptic connections, electrical treatment is a smart and straightforward strategy for brain dysfunction [6], [7].

The deep brain stimulator (DBS), which was approved by the FDA in 1997 [8], has exhibited significant success in treating Parkinson's disease for decades. The DBS module consists of two parts: a long wired electrode array and a palm-sized stimulator body, but these are implanted in the head and clavicle separately owing to the volume limitation. The corresponding surgical process is very complicated and requires an additional surgery within several years to exchange the main module battery. Nevertheless, there is no doubt about its extensive use as a result its overwhelming efficacy [10], [11].

To overcome the above drawbacks, numerous research groups have attempted to reduce the DBS module size by applying wireless powering technologies. Certain authors [12], [13] developed a 1 $cm^3$ miniaturized device and [14] presented a small device that could be injected with a syringe. However, the results had a limited impact in terms of efficacy. Reference [12] evaluated the proposed device through an *in vitro* test, and [14] treated a sciatic nerve, which is much easier than treating a brain. Another approach presented a prototype system and an *in vivo* test with rodent brains [15]–[17]. However, only an electrode array was implanted in the target brain and the remainder of the system was placed outside of the head [16] or on the back [17]. Owing to such technical imperfections, the majority of previous works on DBS inevitably focused on observing the acute neural responses of electrical stimulations. Therefore, EEG/ECoG/EMG signal analysis directly after the stimulation has been a common method for DBS to prove the instantaneous effects. A reliable and convenient DBS platform for long-term tests is urgently required to expand the target applications and verify the sustainability. More specifically, the implant module should be compact for biocompatibility, while the platform should provide a test environment that can easily be

TABLE I
COMPARISON ECBA TO PREVIOUSLY PRESENTED *IN-VIVO* TESTED MINIMALLY INVASIVE NEURAL STIMULATION PLATFORMS

| | [14] | [15] | [16] | [17] | [18] | **This work** |
|---|---|---|---|---|---|---|
| Insertion method | Syringe injection (whole module) | Surgery (microelectrodes) | Surgery (microelectrodes) | Surgery (microelectrodes) | Surgery (whole module) | Surgery (whole module) |
| Target neuron | Sciatic nerve | Brain | Brain | Brain | Brain | Brain |
| Module placing area | Sciatic nerve | Brain (electrode) | Brain (electrode) | Brain (electrode) | Skull | Skull |
| *In vivo* depth | 0.5cm | - | - | 0.8cm | 3cm | 3cm |
| IC size or volume/weight | 0.009mm$^3$ / <1mg | 3.5 × 3.65mm$^2$ | - / 13.8g | 3.06 × 2.53mm$^2$ | 4.4cm$^3$ / 2.79g | 6.48cm$^3$ / 8.69g |
| Package | Silicone | Not considered | Cement | Not considered | Silicone mold | Ti canning |
| Lifetime | Not considered | Not considered | < 3 weeks | Not considered | < 1 month | < 2.5 years |
| Controller | PCB board | PCB | PCB | PCB | Box BS | Helmet BS |
| Subject | Rodent | Rodent | Rodent | Rodent | Canine | Canine |
| Long-term stimulation | N/A | N/A | N/A | N/A | N/A | Available |
| Stimulation efficacy analysis | EMG response (acute) | EEG recording (acute) | - | EEG recording (acute) | EEG recording (acute) | PET-CT(sustained) Histology(inflammatory) |

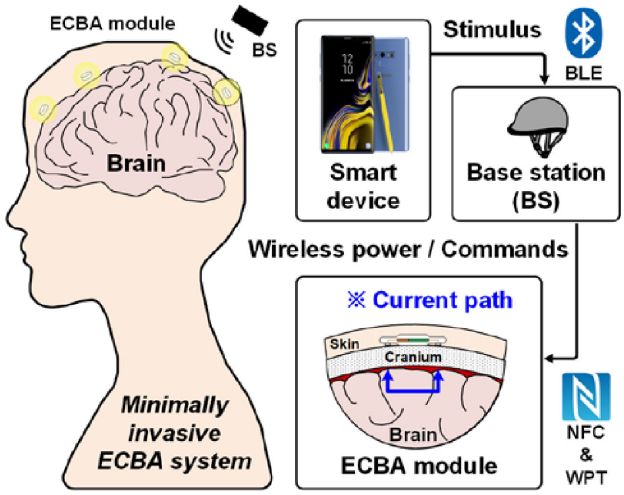


Fig. 1. Concept of proposed ECBA system to support long-term non-anesthetic preclinical studies.

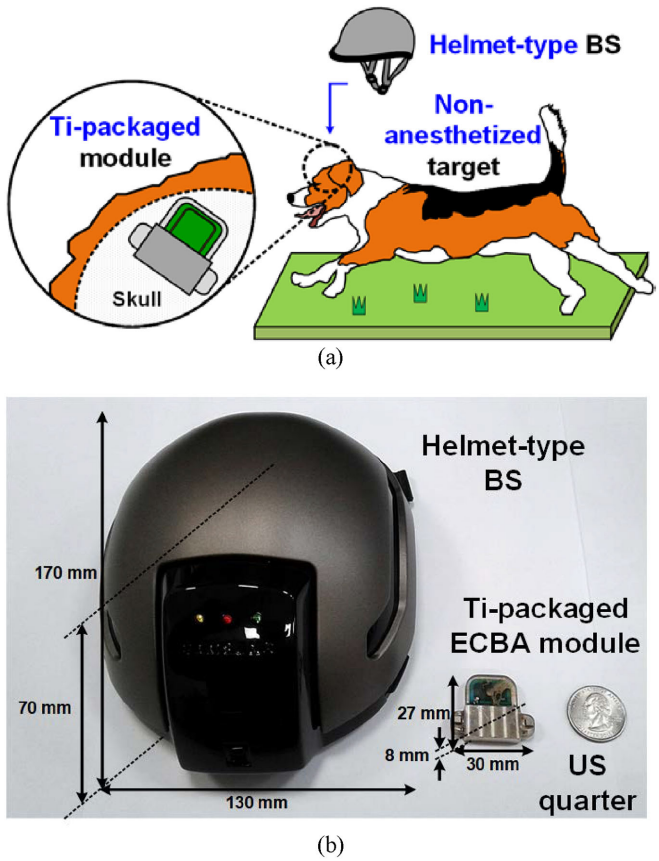


Fig. 2. (a) *In vivo* environment with proposed ECBA system and (b) system component with US quarter for size comparison.

applied to *in vivo* tests on medium-sized subjects such as canines or apes.

Our previous research partially satisfied the requirements for long-term animal studies [18]. We presented a silicone-packaged battery-less miniaturized module and a box-shaped external controller. The charge intensity to the target neuron was 57 times higher than that of transcutaneous direct current stimulation methods [19]. However, this approach exhibited explicit limitations for long-term studies. The silicone packaging only guarantees proper operation for a month and the box-type controller is not suitable for the preclinical studies of moving subjects.

In this work, we presented a new platform known as the Extra-Cranial Brain Activator (ECBA), which is designed for long-term non-anesthetic preclinical studies with canine subjects, as illustrated in Figs. 1 and 2(a). The ECBA system consists of a titanium (Ti)-packaged implant module and a helmet-type base station (BS). By applying the Ti-packaging, the system can operate properly in the *in vivo* environment for more than 2.5 years. Moreover, the helmet-type BS enables *in vivo* experimentation without any restriction on movement. A detailed comparison between the previous works and proposed system is presented in Table I. The table indicates that the ECBA is the only brain stimulation platform that exhibits proven long-term biocompatibility and sustainable stimulation efficacy via radiology analysis. Furthermore, its safety was evaluated via histological analysis by verifying the inflammatory changes in the peri-implanted region. The remainder of this paper is organized as follows: Section II presents an overview of the proposed ECBA system, including its architecture and operation. Section III explains the protocols of the long-term preclinical study using non-anesthetized canine subjects. In Section IV, the *in vivo* measurements are demonstrated through radiology analysis of the PET-CT scan images and histological analysis of

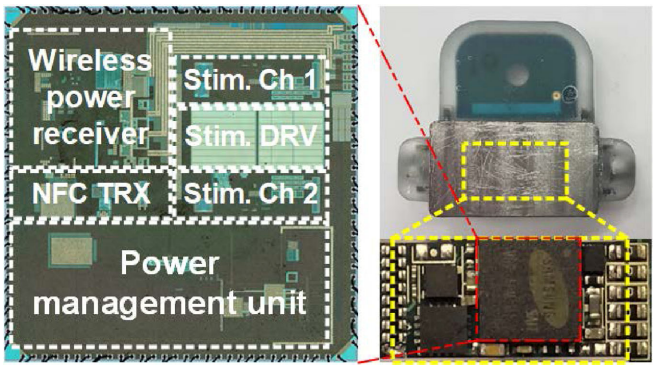


Fig. 3. Microphotograph of customized IC and PCB in the package.

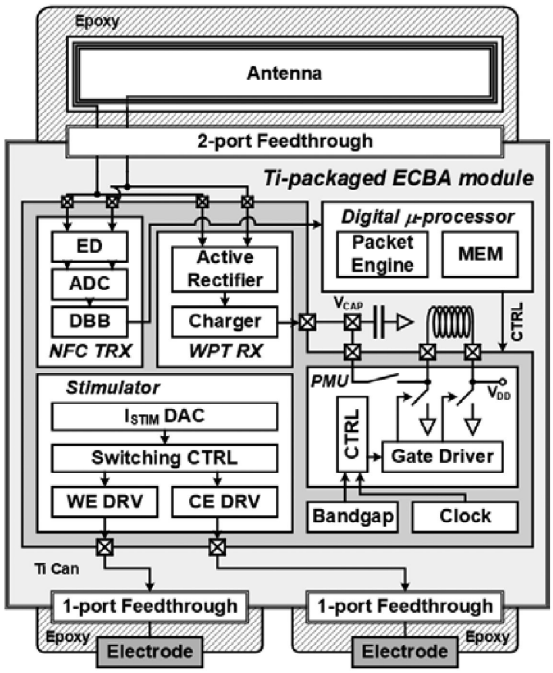


Fig. 4. Architecture of Ti-packaged ECBA module.

brain tissues. The maximum lifetime of the implanted module was also tested under the high temperature aging constraint. Finally, conclusions are provided in Section V.

## II. Implementation of the Proposed ECBA System

### A. Bio-Compatible Ti-Packaged ECBA Module

Fig. 3 displays the core components of the circuit in the ECBA module. In this work, we implemented a customized integrated circuit (IC), including functional blocks: (1) a wireless power receiver (WPRX), (2) a nearfield communication (NFC) transceiver (TRX), (3) a stimulator, and (4) a power management unit (PMU). Two independent stimulation channels were implemented in the proposed IC for wide applicability. The ECBA system used single channel. The entire PCB size was optimized to 75 mm × 15 mm.

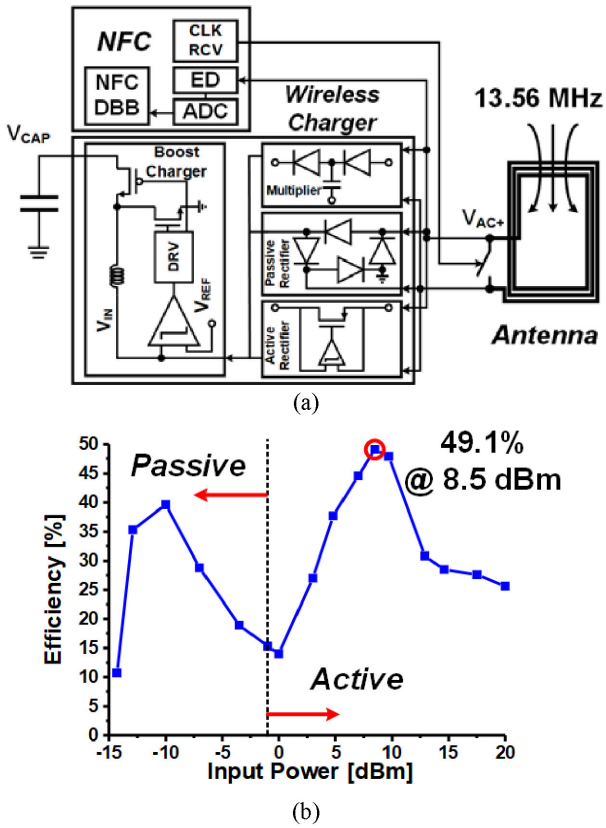


Fig. 5. (a) Circuit diagram of WPRX and (b) measured efficiency.

Fig. 4 presents the overall architecture of the Ti-packaged ECBA module. All components were packaged in a Ti can, except for the antenna and two stimulation electrodes, which were located outside to receive wireless power and induce stimulation pulses, respectively. Epoxy molding was applied to protect the antenna and stimulation electrodes. To connect these components to the main module, feedthroughs [20] with one or two ports were applied, which provided not only hermetic sealing, but also the connection between the circuit and electrodes.

Both the NFC and WPRX used the 13.56MHz band so that they shared a loop antenna. The NFC followed the standard (ISO14443A) compliance. Therefore, the data rate was set to 106 kbps. The length of a packet was only 32 bytes, which included the stimulation parameters and start/end commands. Moreover, the packet was transmitted intermittently, so that 106 kbps allowed for sufficient bandwidth. To reduce the system size, a single-inductor multiple-output converter structure was applied, which required only one inductor for the generation of three different voltages. The main operating voltage of the system was 1.8 V and the compliance voltage of the stimulator was 12 V. An additional 4.2 V was used for the level shifter.

Fig. 5(a) depicts the architecture and performance of the WPRX. Depending on the receiving voltage magnitude, there were two operating modes in the rectifiers: the multiplier/passive and active diode modes. These modes were switched automatically based on the estimation of the input voltage and power level. The boost charger worked when the rectified power was

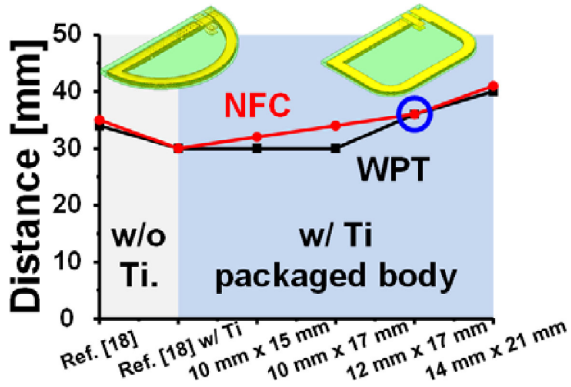


Fig. 6. Maximum distance of NFC (red) and WPRX power transfer (black) depending on different antenna types.

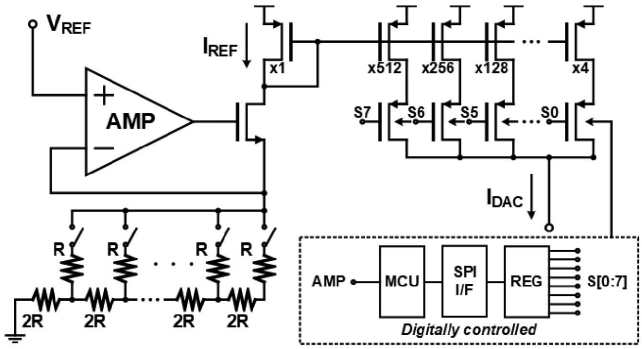


Fig. 7. Circuit diagram of current DAC.

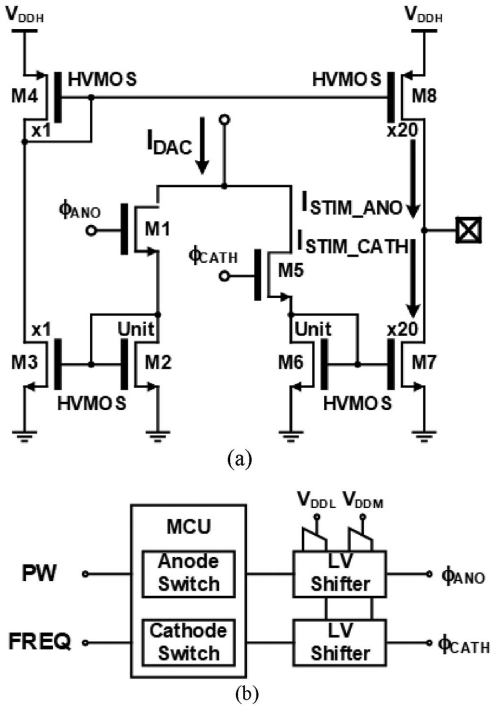


Fig. 8. Circuit diagram of (a) WE DRV and (b) switching CTRL.

sufficiently high to be transferred; otherwise, it entered sleep mode. The overall input power range was measured to -15 dBm to 20 dBm and the maximum charging efficiency was 49% at 8.5 dBm.

The maximum distance guaranteeing the normal operation of the NFC and WPRX functions is described in Fig. 6. According to the graph, when the size of the antenna in the ECBA system was greater than 12 mm $\times$ 17 mm, both performances were better than that of the prototype [18]. As the WPRX electrical function of the prototype was already evaluated by an *in vivo* preclinical test, it was selected as the reference. The reason for the performance degradation was that the Ti disturbed the radiation. Eventually, the size was set to 12 mm $\times$ 17 mm and it was slightly larger than the formal one, namely 7.5 mm $\times$ 15 mm and semicircle shaped.

The stimulator part consisted of a stimulation current ($I_{STIM}$) digital-to-analog converter (DAC), a switching controller (CTRL), and a working/counter electrode driver (WE/CE DRV). As illustrated in Fig. 7, the $I_{STIM}$ DAC first generated a small but very fine and stable reference current, $I_{REF}$, which led to an increase in the stimulation efficiency. The programmable range of $I_{DAC}$ was designed from 1.5625 $\mu$A to 0.4 mA and its amplitude could be adjusted by writing the 8-bit length register, S[7:0].

Fig. 8 presents the circuit diagrams of the $I_{STIM}$ DAC, WE DRV, and switching CTRL. When $I_{DAC}$ was sent from the DAC to the WE DRV, it can be copied in one of two directions: anode or cathode. The direction was selected by switch transistors M1 and M5, controlled by $\phi_{ANO}$ and $\phi_{CATH}$, respectively. The WE DRV consisted of high-voltage components to endure a compliance voltage up to 12 V. High compliance was required to support the injecting or extracting of the desired $I_{STIM}$ through electrodes with high contact impedance. Therefore, the level of the switching pulse voltages, $\phi_{ANO}$ and $\phi_{CATH}$, had to be sufficiently larger than the threshold voltage of the high-voltage switch transistor. As illustrated in Fig. 8(b), the MCU generated switching pulses to allow for programmable stimulation waveforms and the level shifters to convert the voltage level of each switching pulse from $V_{DDL}$ to $V_{DDM}$. As $\phi_{ANO}$ and $\phi_{CATH}$ were never overlapped together, M1 and M5 were closed exclusively. If M1 or M5 was closed, the current mirrors copying $I_{STIM}$ from $I_{DAC}$ ranged from 31.25 $\mu$A to 8 mA. Fig. 9 indicates that the WE DRV can support a constant current up to 4 mA when a contact impedance was less than 1k ohm.

### B. Biocompatible Packaging

It is very important to improve the durability and biocompatibility of the silicone packaging module, which is vulnerable to moisture. Ti, which is a material with excellent biocompatibility, has been used extensively in the field of implantable medical devices [21], [22]. Similarly, medical-grade epoxy is prominent in *in vivo* systems [23], [24]. We demonstrated the durability of the test module using these materials by means of high-temperature accelerated aging tests [25]. To improve the durability and biocompatibility, Ti and epoxy were used as the packaging material for the ECBA module to contact the

TABLE II
STIMULATOR SPECIFICATIONS OF ECBA COMPARED TO PREVIOUSLY PRESENTED *IN VIVO* TESTED NEURAL STIMULATION PLATFORMS

| | | [14] | [15] | [16] | [17] | [18] | This work |
|---|---|---|---|---|---|---|---|
| Technology | | 130nm CMOS | 350nm CMOS | N/A | 180nm CMOS | N/A | 180nm HV CMOS |
| Chip Area | | 0.09 $mm^2$ | 12.775 $mm^2$ | N/A | 7.74 $mm^2$ | 16 $mm^2$ | 2.25 $mm^2$ |
| Core Supply | | 1V | 3.3V | 2.9V, 5.5V | 1V | 3V | 1.8V |
| Compliance | | N/A | N/A | 17.6V | N/A | 18V | 12V |
| # of channels | | 1 | 64 | 1 | 8 | 4 | 2 |
| Stimulation type | | Mono-phasic voltage | Bi-phasic current | Bi-phasic current | Bi-phasic Voltage | Bi-phasic current | Bi-phasic current |
| Power | Standby | - | - | - | | <25μW | <1μW(stand-by) |
| | Bias [a] | - | 2.76μW/ch | 1.9mA (current consumption) | 365μW | 325μW | 170μW (bias) |
| Amplitude (max) | | 38μA | 250μA | 2.036mA | 4.5V | 6.12mA | 8mA |
| Amplitude (unit) | | - | 20μA (min) | 26μA | 93.75mV | 12μA | 31.25μA |
| Pulse-width (max) | | 500μA | - | 100ms | 440μs | 2.55ms | 2.55ms |
| Pulse-width (unit) | | - | - | 500ns | 40μs | 10μs | 10μs |

a) Except the power consumption from the stimulation current

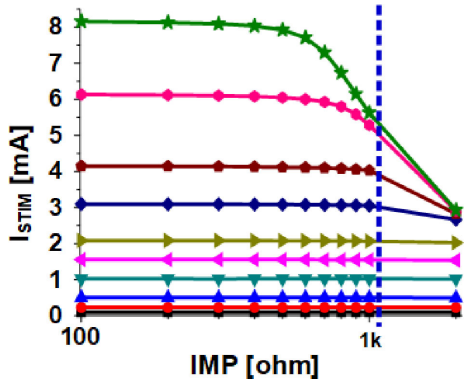


Fig. 9. $I_{STIM}$ driven by WE DRV depending on contact impedance.

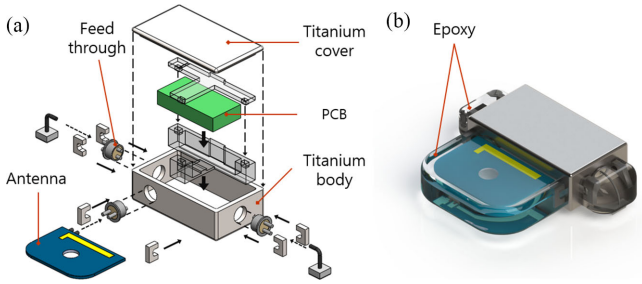


Fig. 10. (a) Schematic of assembly and (b) 3D rendering model.

biological tissues physically. Fig. 10(a) depicts the packaging process including the components of the ECBA module, except for the epoxy shell. The Ti feedthroughs, which could protect the PCB inside the Ti case from moisture penetration, and were interconnected to the antenna and the electrodes located outside the case, were first welded to the case. Thereafter, the Ti case was fully welded to seal both of the electric assembled components, namely the feedthrough and PCB, hermetically. The antenna and electrodes protruding from the Ti can was completely covered with the epoxy (EPO-TEK 301) to ensure insulation as well as hermetic sealing, as shown in Fig. 10(b).

### C. Helmet-Type BS for Long-Term Preclinical Study

As illustrated in Fig. 11(a), the performance of the wireless power transmission between the BS and ECBA module was tested under the body-simulant RF phantom solution prior to the implantation. The antenna of the helmet-type BS had a radius of 80 mm to fit the canine-wearable helmet. It could deliver at least 112.7 mW from the BS to the ECBA module through a path loss of −5.5 dB. This amount of power was sufficient for the normal operation of the ECBA, which consumed less than 9.62 mW on average. As the ECBA module had no battery, the helmet had to be worn at all times during the treatment. The ECBA module could be operated normally if it was placed in the inner circle boundary of the BS antenna. Moreover, if the mutual influence of the coupling between the two was low and the transmitted power was sufficiently high, multiple ECBA modules could be supplied at once. Furthermore, as mentioned at Section II, because we followed the ISO14443 NFC standard including anti-collision protocols, each module had its own ID and could be controlled separately. However, as the sizes of the BS antenna and helmet were designed to fit the head of a canine subject, only a maximum of two or three ECBA modules could be physically placed. In this work, we only placed a single ECBA module on each subject because the main purpose of the experiment was to observe the efficacy of the stimulation. In this manner, we could observe the exact stimulation spot as well as the opposite mirror site of the brain. A small mismatch in the orientation was tolerable. However, if the module was disconnected from the BS antenna, it could not be turned on and the treatment would have to be stopped suddenly. In this case, the handshaking protocol could detect the module's connection. The BS periodically (every 30s) sent the short packet to check the connection and the ECBA module responded with its status. If the connection was lost or the power was not sufficient to drive the stimulation, the yellow LED on the helmet would blink twice per second to alarm the patient. The helmet was designed for a year-old canine subject head, and supported fine adjustment with the lace. Therefore, the BS could be firmly worn by the subject even when the target was not anesthetized as shown in Fig. 12. Moreover, the BS could operate by itself using pre-programmed functions, without communicating with a

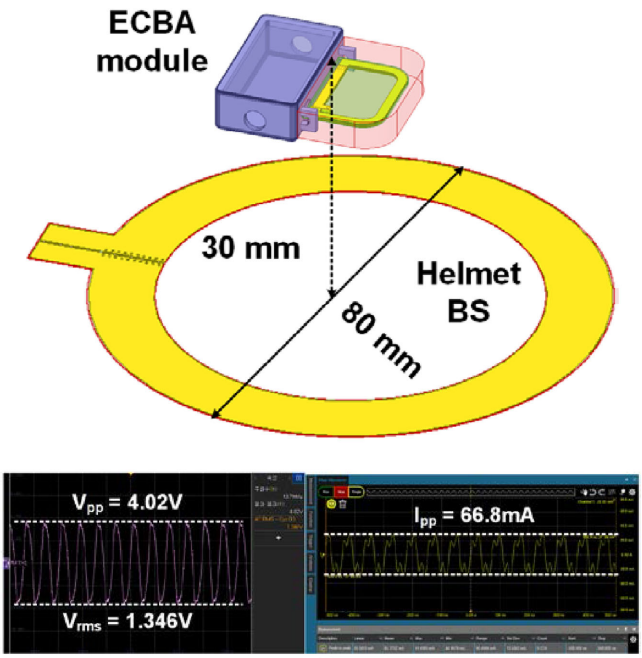


Fig. 11. (a) Power transfer characteristics and (b) test environment with body-simulant RF phantom solution.

Fig. 12. Helmet-type BS applied to non-anesthetized canine subject.

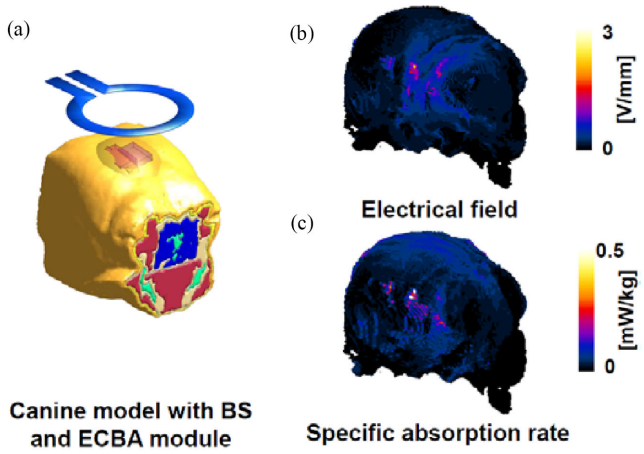


Fig. 13. Simulation for safety of preclinical study protocol with 3D canine model: (a) placement of antenna and ECBA module, as in preclinical study protocol, (b) simulated EF of brain surface, and (c) simulated SAR of brain surface

remote smart device. Prior to the preclinical study, to estimate the safety of the protocol for the brain, simulations were performed using the quasi-static LF solver in Sim4Life (Zurich med tech, Switzerland) to derive the distribution of the specific absorption rate (SAR) and electrical field (EF) induced in the brain under the protocol conditions (stimulation: 40 Hz, WPT: 0.4 W) in a 3-D model imitating the head structure of a beagle (Fig. 13(a)) [26]. In the EF distribution on the brain surface (Fig. 13(b)), the EF was less than 2.5 V/m. Similarly, in the SAR distribution on the brain surface (Fig. 13(c)), the maximum value of the SAR was less than 0.5 mW/kg. These simulated results suggest that our preclinical study protocol was sufficiently stable to not cause damage to the brain tissue [27], [28].

### *D. Smart Device With User Friendly Graphical Interface*

Although the helmet-type BS could start the stimulation protocol by itself, initial programming was required. As indicated in Fig. 14(a), various stimulation waveforms could be programmed by an application on the smart device. Various pulse-based, clinically proven waveforms could be generated with a high degree of freedom as illustrated in Fig. 14(b). The waveform was classified into sets of clusters, trains, and pulses. With the pulse as a base unit, the trains and clusters were adjusted by the numbers and intervals of pulses. The control parameters are displayed in Table III, in which the minimum and maximum values as well as the meaning of each parameter are presented.

## III. In Vivo Preclinical Study Protocols

### *A. Long-Term Non-Anesthetic Stimulation Protocols*

Fig. 15 shows the stimulation protocols of the ECBA system. The stimulation waveforms based on the high-frequency stimulation (HFS) facilitating brain activities [29], [30] are presented in Figs. 15(a) and (c). The activating effect had already been observed in a study monitoring EcoG signals at the same time

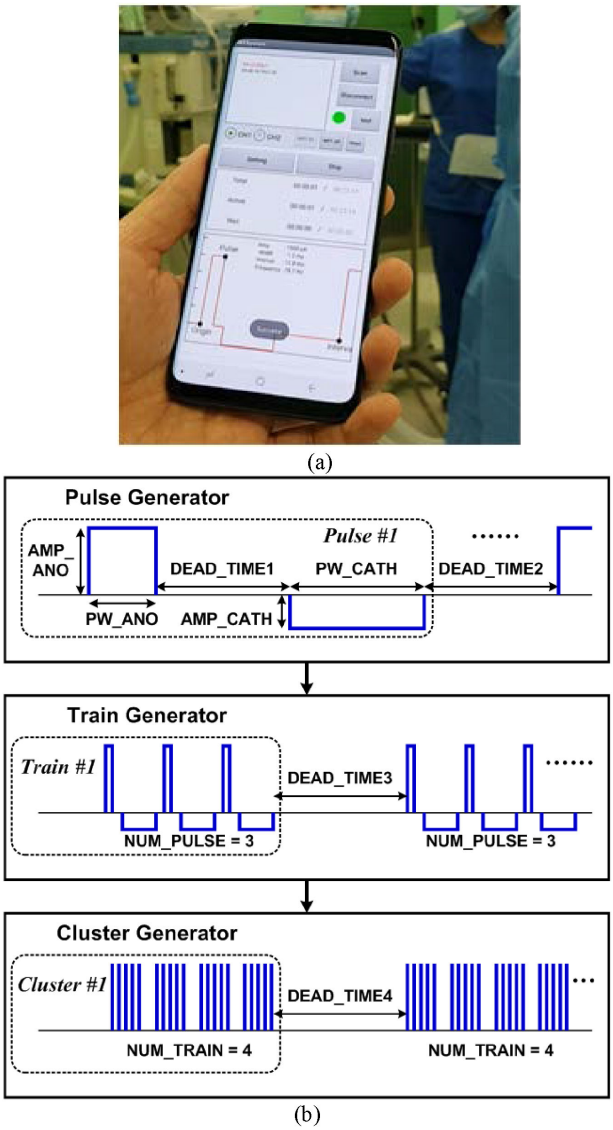


Fig. 14. Programmability of stimulation waveforms.

[18]. According to the reference, the HFS facilitated neural functions, increasing the delta, theta, and alpha regions and decreasing the beta and gamma frequency regions. However, this stimulation efficacy was only observed directly after injection owing to the lack of a long-term preclinical platform.

In this work, the HFS protocol was applied to six canine subjects with a non-anesthetic status, five days a week for four weeks. The subjects were divided into three groups: 1) 10 Hz stimulation, 2) 40 Hz stimulation, and 3) a control group. The control group under went the same experimental protocol wearing the ECBA helmet, but no electrical pulse was injected. An additional beagle, named #0, was used as a pilot model to define the protocols. As illustrated in Figs. 15(a) and (c), both the 10 Hz and 40 Hz HFS waveforms were composed of 30 pulses for a pulse train, and the interval between pulses was 24 s. The amplitude and pulse width of a unit pulse were set to 1.5 mA and 250 $\mu$s, respectively. Stimulation of 30 min were induced twice per day during day and night.

TABLE III
CONTROL PARAMETERS FOR GENERATING STIMULATION WAVEFORMS

| Parameters | Min. | Max. | Note (abbreviation for) |
|---|---|---|---|
| AMP_ANO | 31.25μA | 8mA | Amplitude of anode |
| AMP_CATH | 31.25μA | 8mA | Amplitude of cathode |
| PW_ANO | 10μs | 2.55ms | Pulse width of anode |
| PW_CATH | 10μs | 2.55ms | Pulse width of cathode |
| DEAD_TIME1 | 10μs | 2.55ms | Phase to phase interval |
| DEAD_TIME2 | 80μs | 20.4ms | Pulse to pulse interval |
| DEAD_TIME3 | 40.96ms | 168.83s | Train to train interval |
| DEAD_TIME4 | 20.97s | 23.86h | Cluster to cluster interval |
| NUM_PULSE | 1 | 255 | # of pulses/train |
| NUM_TRAIN | 1 | 255 | # of trains/cluster |
| NUM_CLUSTER | 1 | 255 | # of clusters/therapy |

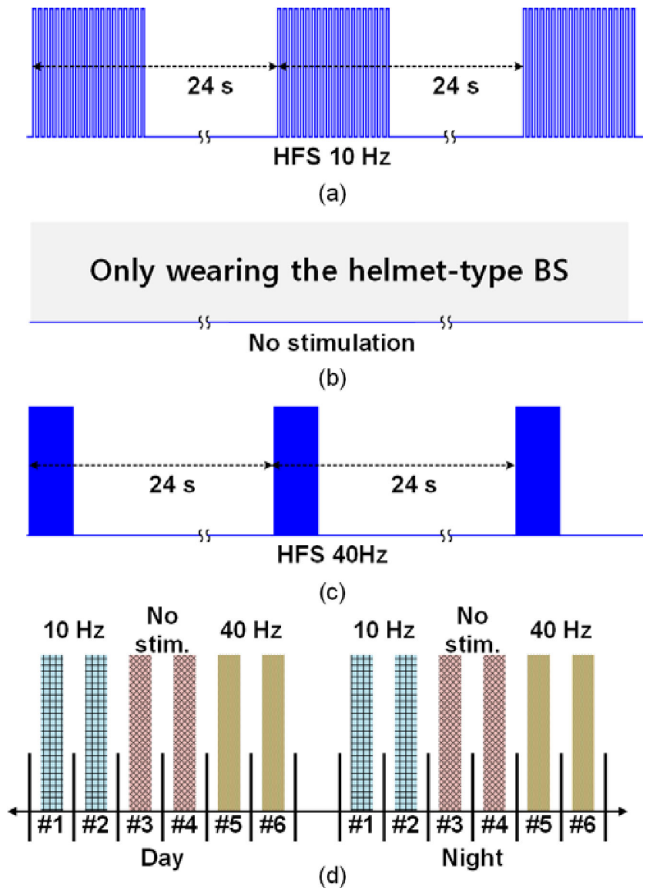


Fig. 15 Stimulation protocols of long-term non-anesthetic preclinical study: (a) 10 Hz, (b) control, and (c) 40 Hz stimulation groups, and (d) daily stimulation time slots for six subjects over four weeks.

### *B. Data Analysis Protocols After Long-Term Stimulation*

First, an MRI scan was conducted on the pilot subject #0 to verify the quality of the scanned images for evaluating changes before and after the stimulation. However, as indicated in Fig. 16, the images were distorted owing to the Ti, so that it was difficult to monitor the changes, especially near the region of the implantation of the ECBA module, which was the most important spot. Hence, we obtained PET-CT scan images of the six main subjects to demonstrate the efficacy of the long-term stimulation. A PET-CT scan was conducted three times for each subject. The

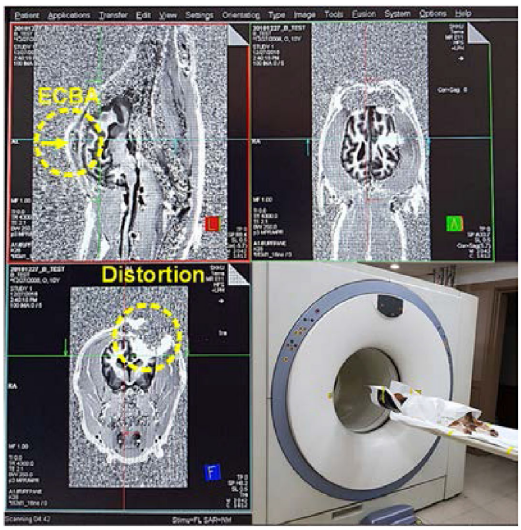


Fig. 16. MRI images after implantation of ECBA module (#0, pilot subject, sliced plane).

first two were conducted one week before and one week after the stimulation protocol to observe immediate changes. The final one was conducted three months after the end of the protocol to monitor the sustainability of the efficacy.

The PET-CT scans were performed using the Siemens Biograph 6 (Siemens, Germany) at the baseline before and after the protocol. All subjects were injected with a dose of 18F-FDG at 2.5 mCi. After 30 min of resting time, PET-CT imaging was performed for 20 min under anesthesia. All individual datasets in the DICOM format obtained by the PET-CT image acquisition were converted into NIfTI format using the DCM2NII software (https://www.nitrc.org/projects/dcm2nii/). Brain masking was performed manually using the MRIcro software (https://www.mccauslandcenter.sc.edu/crnl/mricro) after removing the skull from the CT image for each subject based on the extracted NIfTI format prior to image processing. The PET data with artifacts removed excluding the brain area were reoriented based on the data of subject #1 using the SPM software (https://www.fil.ion.ucl.ac.uk/spm/software/spm12/). The images of all subjects (voxel size: 0.488 mm $\times$ 0.488 mm $\times$ 1.500 mm; matrix: 512 $\times$ 512 $\times$ 109) were rigidly co-registered to the data of subject #1 for comparative analysis using the FSL software (https://fsl.fmrib.ox.ac.uk/fsl/fslwiki/). To analyze the relative pre- and post- brain stimulation, all of the data were normalized to a z-score and the glucose metabolism change was calculated. Further image processing was performed through SPM12 by applying the averaged symmetric canine brain template parcellated as functional regions of the brain to the PET images for the purpose of reliable structural analysis [31]. The PET scan images and MR image (#1) that were manually extracted using MRIcron were co-registered to the canine template (voxel size: 0.5 mm $\times$ 0.5 mm $\times$ 0.5 mm; matrix: 221 $\times$ 241 $\times$ 257). Similarly, the PET data were spatially normalized to the template, after segmenting the MR image in the provided tissue probability map. The normalized images in the template were analyzed according to the labeled region of interest (ROI).

### C. Histopathological Assessment Around ECBA in Scalp Tissue and Underlying Brain Areas of Beagles

The biocompatibility was evaluated by means of a histopathological analysis after completing the *in vivo* experiment. Following 17 months of implantation of the ECBA, two beagles (#1, #6), were euthanized and the tissues surrounding the device, including the scalp, calvarium, and underlying brain regions thereof were examined. Furthermore, a subsequent postmortem histological examination was performed, as illustrated in Fig. 20(a). Prior to the histological analysis, *ex vivo* tissues were fixed in 4% paraformaldehyde immediately following the necropsy. The histological analysis was performed with hematoxylin and eosin (H&E) staining to evaluate the stimulation-induced changes in the neuronal integrity of the brain tissues.

### D. High-Temperature Accelerated Method

Arrhenius' law, which suggests that the degradation rate changes with the temperature T, is widely applied to studies that evaluate the durability of various materials [32]. To verify the durability further, an aging test with high temperature acceleration was performed on the extracted ECBA module after 17 months of implantation. During the aging test, the pulse output from the ECBA module was gathered, with the same patterns that were applied to the preclinical study protocol, and the duration until the functional degradation reached over 10% was measured. The module could malfunction as a result of moisture invasion. The constant temperature bath was filled with a solution of pH 7.4 and was adjusted by diluting phosphate buffered saline (PBS) in deionized water to simulate *in vivo* physiological conditions. The PBS solution maintained 76 with an acceleration factor of 15 according to the Arrhenius equation based on a body temperature of 37.5. The distance between the external antenna and ECBA module placed in the water bath was set to 1.0 cm. The ECBA system, which was subjected to an additional sealing process, was connected to an insulated wire leading out of the bath that was capable of measuring the device output. The voltage that was applied through the load resistance (50 ohm) connected to the insulated wire was measured using a DAQ system (cDAQ-9174, National Instruments, USA) that was controlled by the LabVIEW software (National Instruments, USA) under the condition of a 40 Hz stimulation parameter (amplitude: 1.5 mA, pulse width: 250 $\mu$s, frequency: 40 Hz).

## IV. In-Vivo Measurement Results

### A. Diagnostic Radiology Analysis With PET-CT Scan

Fig. 16(a) indicates that the ECBA was inserted over the skull of the right hemisphere based on the top of the canine subject's head. Fig. 16(b) depicts the relative changes in the glucose metabolism in the coronal plane, which was prominent on brain activation in the region adjacent to the implanted ECBA module. The relative brain activation increased in the middle part of the brain in the 10 Hz group (#1, #2). Strong glucose metabolism changes were observed in the region under the module and in the mirror site in the 40 Hz group (#5, #6). No remarkable changes were observed in the control group (#3, #4). Consequently, the

TABLE IV
EXPERIMENTAL DATES OF EACH TASKS TO PROVE EFFICACY OF LONG-TERM PRECLINICAL TEST WITH PROPOSED ECBA SYSTEM (YY/MM/DD)

| Canine models | MRI before implant | Implant | MRI after implant | PET-CT pre-stim. | PET-CT post-stim. | | Stimulation period[a)] | Sacrifice (euthanasia) | Total implanted period |
|---|---|---|---|---|---|---|---|---|---|
| | | | | | First | Second | | | |
| #0 (pilot) | 18/9/19 | 18/10/10 | 18/12/27 | 19/1/7 | - | - | - | 19/4/17 | 6.3 months |
| #1 | 18/10/31 | 18/11/7 | - | 19/3/11 | 19/4/15 | 19/7/15 | 19/3/18 ~ 19/4/12 | 20/3/13 | 14.5 months |
| #2 | 18/10/31 | 18/11/7 | - | 19/3/11 | 19/4/16 | 19/7/16 | 19/3/18 ~ 19/4/12 | 20/7/22 | 20.8 months |
| #3 | 18/10/31 | 18/11/28 | - | 19/3/12 | 19/4/17 | 19/7/17 | 19/3/18 ~ 19/4/12 | 20/4/19 | 16.9 months |
| #4 | 18/11/2 | 18/11/28 | - | 19/3/12 | 19/4/17 | 19/7/15 | 19/3/18 ~ 19/4/12 | 20/4/19 | 16.9 months |
| #5 | 18/11/2 | 18/12/5 | - | 19/3/13 | 19/4/15 | 19/7/15 | 19/3/18 ~ 19/4/12 | 20/7/22 | 19.8 months |
| #6 | 18/11/2 | 18/12/5 | - | 19/3/13 | 19/4/16 | 19/7/16 | 19/3/18 ~ 19/4/12 | 20/3/13 | 15.5 months |

a) Experiments were conducted only on working days (Monday to Friday)

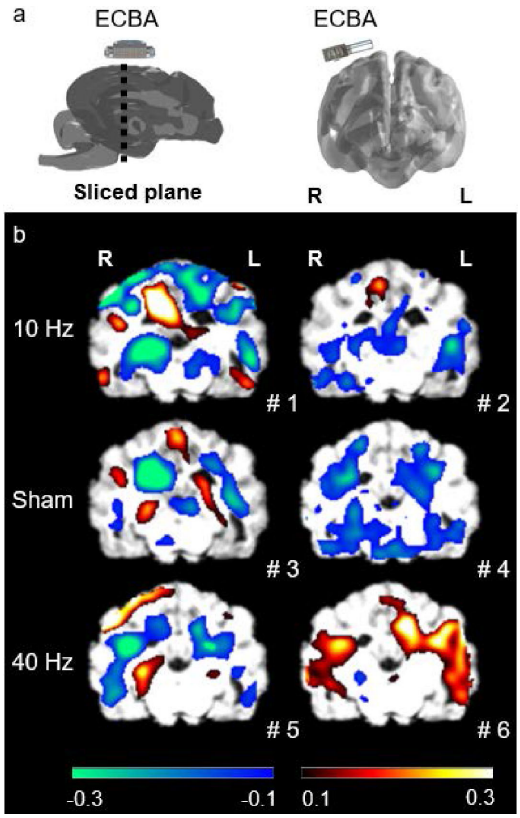


Fig. 17. (a) Position of implanted ECBA in brain at sagittal and coronal views, (b) PET-CT scan of all subjects (#1 to #6) where ECBA was located in coronal plane in (a).

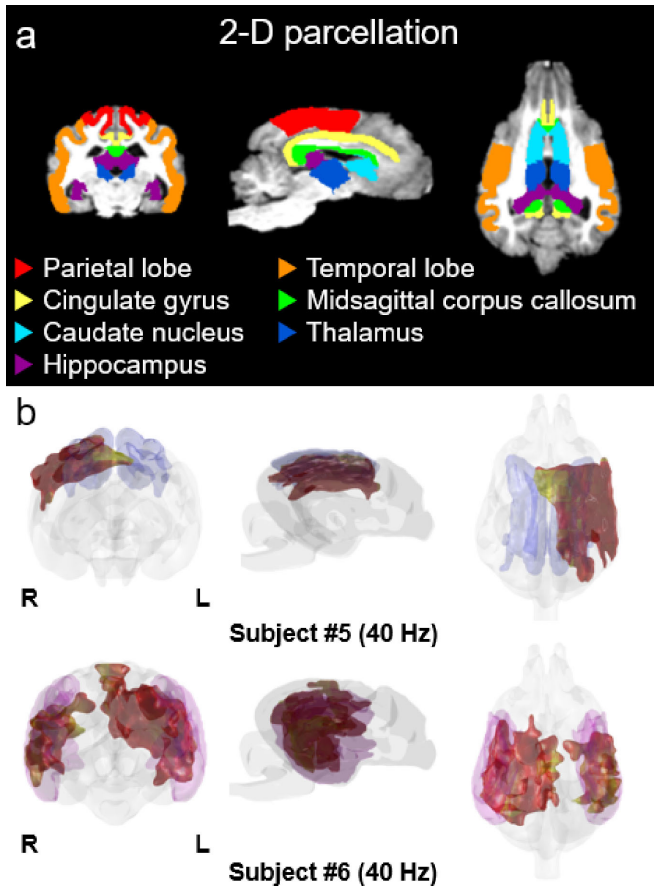


Fig. 18. (a) Two dimensional parcellation of seven regions from location of ECBA module to deep areas of brain based on averaged canine template, (b) 3D images of brain activation (#5: red, #6: red) of 40 Hz group to compare expected activation areas (parietal lobe: blue, temporal lobe: purple).

40 Hz group exhibited the highest efficacy on brain activation. To compare the activity owing to the classified brain regions based on the PET-CT results, seven regions were parcellated from those nearest the parietal lobe to the hippocampus in order of distance, as presented in Fig. 17(a).

The activation areas were focused on the parietal lobe and temporal lobe, which are the cortical regions of the brain. Fig. 17(b) indicates that the active region of subject #5 (red) was overlapped on the right side of the parietal lobe (blue), whereas the active region of subject #6 (red) was overlapped on the left side of the temporal lobe (purple). This result verified that the HFS affected the activation of the cortical regions adjacent to the ECBA module.

The tendencies of the brain activation according to the aforementioned stimulus were clearly revealed in the numerical analysis of the brain regions. Fig. 19 presents graphs of the calculated maximum change value of the relative glucose metabolism in the seven ROIs, listed by distance from the ECBA, in all subjects. As illustrated in Fig. 19(a), the activation of the region close to the ECBA in the 40 Hz group was higher than in the other groups.

In particular, the maximum value was 1.03 in subject #5 and 1.36 in subject #6, whereas, the value was lower than 0.35 in

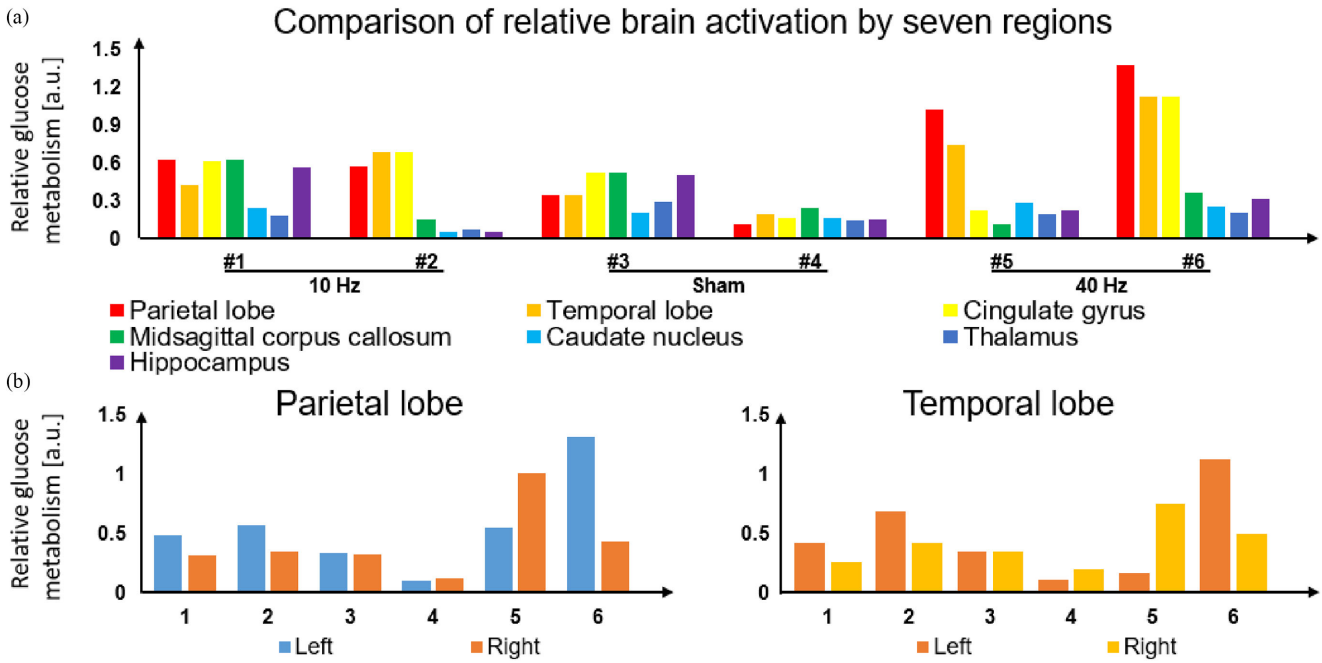


Fig. 19. (a) Maximum changes in relative glucose metabolism [arbitrary unit, a.u.] of pre- and post-stimulation protocols among seven brain regions, was listed in order of distance from ECBA, in all subjects and (b) graph dividing two regions (parietal and temporal lobes) prominent in 40 Hz group into left and right hemispheres.

the control group in the case of the parietal lobe. The control group value was lower than 0.35 in the case of the temporal lobe, whereas the maximum value was 1.12 in the subject #6. Fig. 19(b) indicates that the graph expressed each maximum value by dividing the left and right hemispheres of the parietal lobe and temporal lobe. The maximum value of the right hemisphere in the parietal lobe was 1.00, which was greater than the value of 0.544 in the left hemisphere in the parietal lobe of subject #5. The value of 0.75 in the right hemisphere in the temporal lobe was more than 4 times larger than the left value. In contrast, the maximum values were greater than 1.12 in both areas, which was more than twice the value on the right in subject #6, as the mirror site was activated. Thus, according to the analysis, the HFS enhanced the activity of the parietal and temporal lobes associated with memory and sensory abilities.

### *B. Long-Term Safety of ECBA According to Histological Evaluation*

After 17 months of the *in-vivo* experiment, two subjects, (#1, #6), were euthanized for a histological examination. One was from the 10 Hz group and the other was from the 40 Hz group. The main purpose of the histological analysis was to confirm the safety in terms of the physical effects of the device implantation and electrical effects of the HFS waveforms. To assess microscopic signs of damage caused by prolonged contact with the ECBA, a sagittal sectioning of the scalp traversing the contact areas was performed in both hemispheres, as shown in Fig. 20(a). As expected, the findings demonstrated the chronic inflammatory changes in areas that contacted with the device, consisting of predominantly monocytes and lymphocytes, as well as several granulation tissues with fibrous capsules adjacent to the inflammatory tissues, as illustrated in Fig. 20(b), (c) and (d).

However, we could not observe any other histopathological changes in the right region of the brain underlying the ECBA, including the parietal cortical section, white matter, and underlying hippocampal tissues, as indicated in Figs. 21(a), (e), (c), and (g), compared to the left regions of the brain, as indicated in Figs. 21(b), (d), (f) and (h), thereby confirming the long-term safety of the chronic ECBA stimulation protocols.

### *C. Device Durability With Aging Test*

The aging test performed over 30 days measured the pulses released from the ECBA module three times every two days. The tested ECBA module was retrieved from subject #3, at which stage it had already experienced approximately 17 months in the real implantation environment. Fig. 22(a) presents the graph of the overlapped pulses selected every two weeks (14 and 28 days), including the results of the first day (0 days). The measurement value (1.52 mA) on day 0 matched the amplitude (1.50 mA) of the programmed stimulation parameters. The amplitude decreased slightly on the 14th day and the pulse was noticeably attenuated on the 28th day, whereas the frequency or pulse width remained consistent. Fig. 22(b) presents the averages of the amplitudes from all data sets normalized to the mean of the first results. The results demonstrated that the pulse amplitude decreased continuously over time in the accelerated test environment. a pulse amplitude of 0.95 or more was released from the device until the 28th day, whereas the amplitude on the 30th day was rapidly reduced to less than 90% at 0.89. The expected

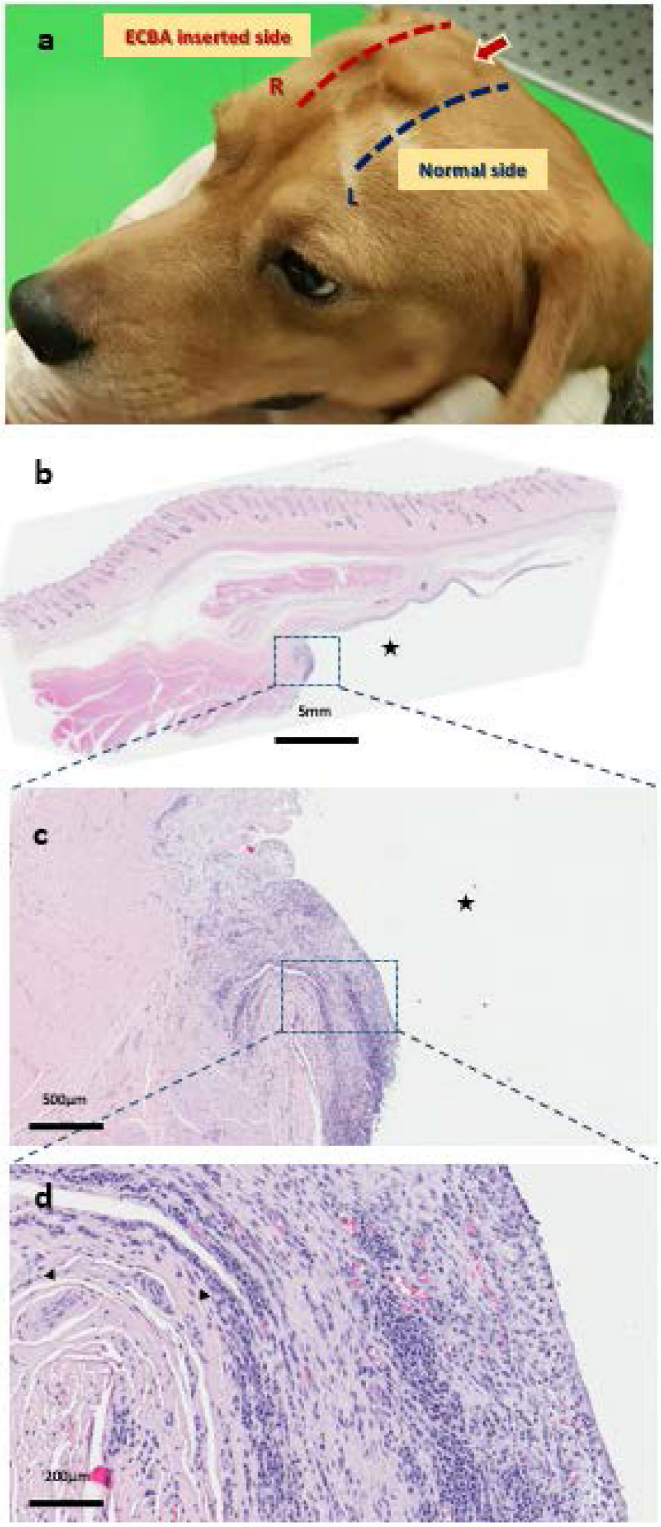


Fig. 20. (a) Photograph of beagle in which ECBA module was inserted in right parietal area and well sustained for $>$ 1 year. The dotted lines designate the incision lines for the tissue preparation after euthanasia. (b) and (c) Histological images of sagittal section traversing contact areas of ECBA in right hemisphere with covering subcutaneous surface. The asterisk ($\star$) indicates the region where the ECBA was placed. (d) Magnified microscopic imaging of slide C demonstrating chronic inflammatory phase consisting of predominantly monocytes and lymphocytes, and granulation tissues subsequently leading to well-organized fibrous capsules ($\Delta$) adjacent to inflammatory tissues.

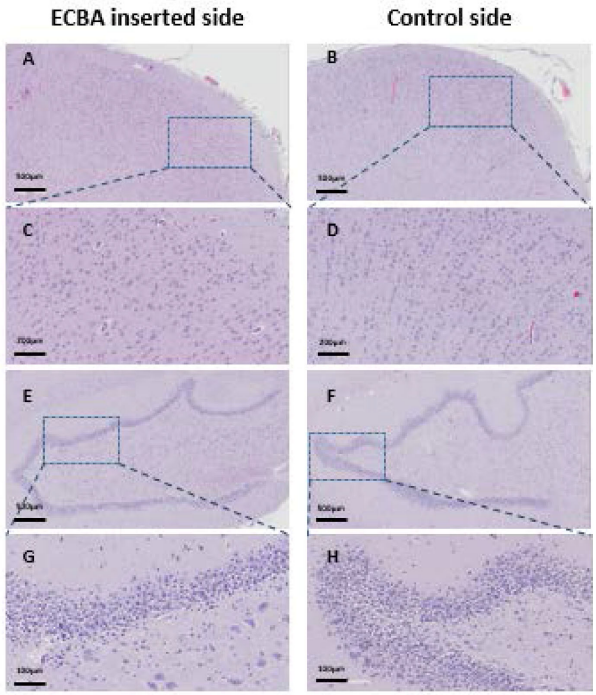


Fig. 21. Microscopic images of brain sagittal sections underneath the ECBA (A, C, E, G: right side) and at normal hemisphere (B, D, F, H: left side by H&E staining). Representative histological slice demonstrating absence of cortical defect on right side with ECBA (A) as well as control side (B). Representative image of magnified cortical pyramidal cells with an intact laminar architecture in both sides (C, D). Likewise, hippocampal slices demonstrate the absence of hippocampal cellular damage on the side where ECBA was inserted (E, G), as well as control side (F, H).

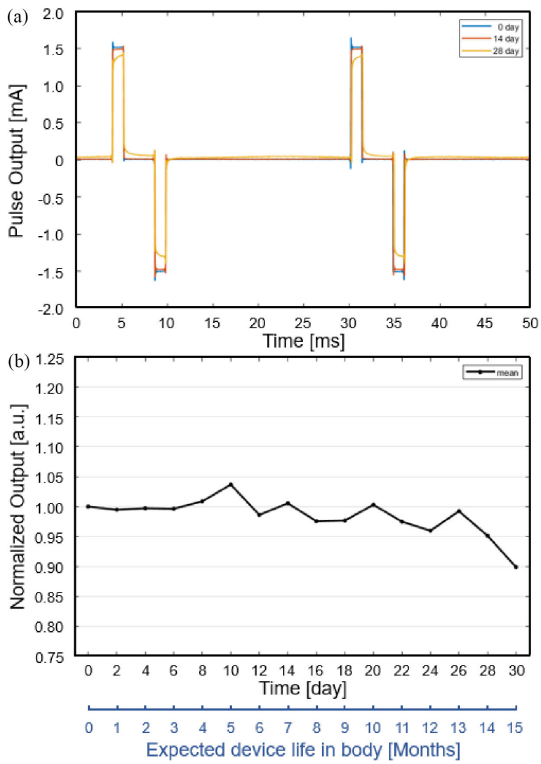


Fig. 22. (a) Graph of overlapped pulses measured every 2 weeks from start date (0, 14, and 28 days) in accelerated conditions (pH : 7.4, temperature : 76.0), and (b) graph normalized by dividing mean current on the first day by all data.

life of the ECBA under *in vivo* conditions was 14 months, as guaranteed by the high-temperature accelerated aging testing. As a result, durability up to 31 months was guaranteed according to 17 months under the experimental conditions and 14 months under the aging test conditions.

## V. Conclusion

The ECBA has been presented, which is the first complete system of an implantable platform for long-term non-anesthetic preclinical studies. This system consists of a biocompatible Ti-packaged battery-less implantable module, a helmet type BS that powers the module wirelessly, and a smart mobile device that communicates with the BS for remote control.

The ECBA provides various stimulation waveform patterns including clinically proven ones. In this work, six canine subjects were divided into three groups of two each. The three groups were exposed to 10 Hz stimulation, 40 Hz stimulation, and no stimulation, twice daily, five days a week for four weeks. Both the 10 Hz and 40 Hz stimulation groups underwent a predetermined 30 min of stimulation protocols, whereas the control group (no stimulation) underwent the exact same experiment protocol wearing the ECBA helmet, but with no electric pulse actually injected.

The clinical effects were evaluated by analyzing PET-CT scan images and monitoring the glucose metabolism changes in the brain after injecting 18F-FDG into the subjects. An increase in the glucose metabolism was detected in the 10 Hz and 40 Hz stimulation groups, whereas no specific change was observed in the control group. More specifically, the 10 Hz stimulation group exhibited relative increase in brain activation in the middle part of the brain, whereas the 40 Hz stimulation group exhibited strong glucose metabolism at two locations, the area beneath the ECBA module and its symmetric area of the brain.

The biocompatibility and safety of the ECBA were also thoroughly examined by means of a histological analysis and a high-temperature aging test. For the histological analysis, each subject in both stimulation groups was euthanized after 17 months of the *in vivo* experiment. The analysis confirmed no histopathological change in the right region of the brain where the ECBA was placed, including the parietal cortex, white matter, and underlying hippocampal tissues. The longevity of the ECBA was further evaluated via a high-temperature aging test directly after 17 months of the *in vivo* experiment. The test with an acceleration factor 15 demonstrated 14 additional months of life time, which confirmed at least 2.5 years of safe operation.

In summary, we completed the first brain implant system for long-term animal studies and established meaningful biomedical results that would not have been possible without this platform.

## VI. Further Works

In this work, there were only two subjects per observed group, which can statistically be considered an insufficient number to generalize the efficacy of the treatment. However, other works have also reported *in vivo* results with two animal subjects for each active group [33], [35]. Although we conducted our experiment using only two subjects per group, we clearly obtained coherent and positive results from each subject, which demonstrated the reliability of our data. However, we agree that the number of subjects was insufficient. Thus, as our next step, we plan to conduct additional behavior experiments on more than 10 subjects at the same time, to monitor the actual enhancement of the memory and cognitive skills.

## References


[1] K. Famm, B. Litt, K. J. Tracey, E. S. Boyden, and M. Slaoui, "Drug discovery: A jump-start for electroceuticals," *Nature*, vol. 496, pp. 159–161, Apr. 2013.

[2] Markets and Markets. "Electroceuticals/Bioelectric medicine market: Global forecast to 2021," Report code: MD 4358, 2016, [Online] Available: https://www.marketsandmarkets.com/Market-Reports/electroceutical-market-222053956

[3] S. Miochinovic, S. Somayajula, and S. Chitnis, "History, applications, and mechanisms of deep brain stimulation," *J. Amer. Med. Assoc., Neurol.*, vol. 70, no. 2, pp. 163–171, Feb. 2013.

[4] H. Kassiri *et al.*, "Closed-loop neurostimulators: A survey and a seizure-predicting design example for intractable epilepsy treatment," *IEEE Trans. Biomed. Circuits Syst.*, vol. 11, no. 5, pp. 1026–1040, Oct. 2017.

[5] W. Chen *et al.*, "A fully integrated 8-channel closed-loop neural-prosthetic CMOS SoC for real-time epileptic seizure control," *IEEE J. Solid-State Circuits*, vol. 49, no. 1, pp. 232–247, Jan. 2014.

[6] F. Pulvermüller, "How neurons make meaning: Brain mechanisms for embodied and abstract-symbolic semantics," *Trends Cogn. Sci.*, vol. 17, no. 9, pp. 458–470, Sep. 2013.

[7] S. G. Hormuzdi, M. A. Filippov, G. Mitropoulou, H. Monyer, and R. Bruzzone, "Electrical synapses: A dynamic signaling system that shapes the activity of neuronal networks," *Biochim. Biophys. Acta Biomembr.*, vol. 1662, no. 1–2, pp. 113–137, Mar. 2013.

[8] J. Gardner, "A history of deep brain stimulation: Technological innovation and the role of clinical assessment tools," *Soc. Stud. Sci.*, vol. 34, no. 5, Oct. 2013.

[9] in *Product Manual for Activa PC Medtronic*. Medtronic Parkway, Minneapolis, MN, USA, pp. 1–18, 2008. [Online]. Available: https://www.medtronic.com

[10] A. M. Lozano *et al.*, "Deep brain stimulation: Current challenges and future directions," *Nat. Rev. Neurol.*, vol. 15, no. 3, pp. 148–160, Jan. 2019.

[11] L. Pycroft, J. Stein, and T. Aziz, "Deep brain stimulation: An overview of history, methods, and future developments," *Brain Neurosci. Adv.*, vol. 2, pp. 1–6, Dec. 2018.

[12] D. Rozgić *et al.*, "A 0.338 cm3, artifact-free, 64-contact neuromodulation platform for simultaneous stimulation and sensing," *IEEE Trans. Biomed. Circuits Syst.*, vol. 13, no. 1, pp. 38–55, Feb. 2019.

[13] C. Kim *et al.*, "A 3 mm × 3 mm fully integrated wireless power receiver and neural interface system-on-chip," *IEEE Trans. Biomed. Circuits Syst.*, vol. 13, no. 6, pp. 1736–1746, Dec. 2019.

[14] A. Khalifa *et al.*, "The microbead: A 0.009 mm3 implantable wireless neural stimulator," *IEEE Trans. Biomed. Circuits Syst.*, vol. 13, no. 5, pp. 971–985, Oct. 2019.

[15] R. Shulyzki *et al.*, "320-channel active probe for high-resolution neuromonitoring and responsive neurostimulation," *IEEE Trans. Biomed. Circuits Syst.*, vol. 9, no. 1, pp. 34–49, Feb. 2015.

[16] F. Kölbl *et al.*, "An embedded deep brain stimulator for biphasic chronic experiments in freely moving rodents," *IEEE Trans. Biomed. Circuits Syst.*, vol. 10, no. 1, pp. 72–84, Feb. 2016.

[17] Y. Lin *et al.*, "A battery-less, implantable neuro-electronic interface for studying the mechanisms of deep brain stimulation in rat models," *IEEE Trans. Biomed. Circuits Syst.*, vol. 10, no. 1, pp. 98–112, Feb. 2016.

[18] H. Lee *et al.*, "Development of wirelessly powered, extracranial brain activator (ECBA) in a large animal model for the future non-invasive human neuromodulation," *Sci. Rep.*, vol. 9, Jul. 2019, Art. no. 10906.

[19] in *Product Manual for Programmable Direct Current Stimulator, Neuro Care*. Rindermarkt, Munich Germany, 2018, pp. 1–2. [Online]. Available: https://www.neurocaregroup.com

[20] in *Product Manual for Standard Bi-polar Feedthrough, Morgan Advanced Materials*. Theodore Rice Blvd, New Bedford, MA,USA. [Online]. Available: https://morganadvancedmaterials.com

[21] F. Froes and M. Qian, in *Titanium in Medical and Dental Applications*. Cambridge, U. K.: Woodhead Publishing, 2018.

[22] M. Kaur and K. Singh, "Review on titanium and titanium based alloys as biomaterials for orthopaedic applications," *Mater. Sci. Eng. C*, vol. 102, pp. 844–862, Sep. 2019.

[23] A. Phan *et al.*, "A wireless handheld pressure measurement system for in vivo monitoring of intraocular pressure in rabbits," *IEEE Trans. Biomed. Eng.*, vol. 67, no. 3, pp. 931–937, Mar. 2020.
[24] E. S. Cadel, L. L. Frazer, E. D. Krech, K. J. Fischer, and E. A. Friis, "Analysis of how compliant layers and encapsulation affect power generated from piezoelectric stacked composites for bone healing medical devices," *J. Biomed. Mater. Res. A*, vol. 107, no. 12, pp. 2610–2618, Dec. 2019.
[25] W. Kang, J. Kim, S. Jang, and S. Park, "Department of semi-permanent package and performance verification system for electroceuticals research," Korean Society for Biomedical Engineering, pp. 318–319, May 10, 2019. [Online]. Available: http://www.kosombe.or.kr/file/2019_spring_191104.pdf
[26] W. Kang *et al.*, "Analyzing the advantages of subcutaneous over transcutaneous electrical stimulation for activating brainwaves," *Sci. Rep.*, vol. 10, pp. 1–14, Apr. 2020, Art. no. 7360.
[27] M. R. Awal, M. Jusoh, M. R. C. Beson, T. Sabapathy, M. Kamarudin, and M. R. Basar, "Frequency restrictions for wireless power transfer of implantable medical devices," *ARPN J. Eng. Appl. Sci.*, vol. 10, no. 19, pp. 8707–8714, 2015.
[28] International Commission on Non-Ionizing Radiation Protection. "Guidelines for limiting exposure to time-varying electric and magnetic fields (1 hz to 100 kHz)," *Health Phys.*, vol. 99, no. 6, pp. 818–836, Dec. 2010.
[29] S. H. Doeltgen and M. C. Ridding, "Low-intensity, short-interval theta burst stimulation modulates excitatory but not inhibitory motor networks," *Clin. Neurophysiol.*, vol. 122, no. 7, pp. 1411–1416, Jul. 2011.
[30] S. Zaghi, M. Acar, B. Hultgren, P. S. Boggio, and F. Fregni, "Noninvasive brain stimulation with low-intensity electrical currents: Putative mechanisms of action for direct and alternating current stimulation," *Neuroscientist*, vol. 16, no. 3, pp. 285–307, 2010.
[31] B. Nitzsche *et al.*, "A stereotaxic breed-averaged, symmetric T2w canine brain atlas including detailed morphological and volumetrical data sets," *NeuroImage*, vol. 187, pp. 93–103, Feb. 2019.
[32] L.-R. Bao and A. F. Yee, "Effect of temperature on moisture absorption in a bismaleimide resin and its carbon fiber composites," *Polymer*, vol. 43, no. 14, pp. 3987–3997, Jun. 2002.
[33] J. A. Araujo, N. H. Greig, D. K. Ingram, J. Sandin, C. de Rivera, and N. W. Milgram, "Cholinesterase inhibitors improve both memory and complex learning in aged beagle dogs," *J. Alzheimers Dis.*, vol. 26, no. 1, pp. 143–155, 2011.
[34] A. Jezzini, S. Rozzi, E. Borra, V. Gallese, F. Caruana, and M. Gerbella, "A shared neural network for emotional expression and perception: An anatomical study in the macaque monkey," *Front. Behav. Neurosci.*, vol. 9, no. 243, pp. 1–17, 2015.
[35] P. Yang *et al.*, "Neuromodulation of sensory networks in monkey brain by focused ultrasound with MRI guidance and detection," *Sci. Rep.*, vol. 8, May 2018, Art. no. 7993.

**Hyungwoo Lee** (Member, IEEE) received the B.S., M.S. and Ph.D. degrees in electrical engineering from the Korea Advanced Institute of Science Technology, Daejeon, South Korea, in 2010, 2012 and 2015, respectively. From 2015, he has been with Samsung Advanced Institute of Technology, Suwon, Korea, as a Research Staff Member. His current research interests include ultra-low energy circuit and system design for implantable medical applications and the neuromorphic processor design including an analog in-memory computer.

**Jun Seung Mun** received the B.S. degree in mechanical engineering from the Pohang University of Science and Technology, Pohang, South Korea, in 2017. He is currently working toward the Ph.D. degree as M.S. and Ph.D. candidate with Innovative Medical Solution Lab., the Pohang University of Science and Technology, Pohang, South Korea. His current research interests include implantable medical device and closed loop portable neurostimulation system.

**Woo Ram Jung** received the B.S. and M.S. degrees in biology from Sungkyunkwan University, Seoul, South Korea, in 2006 and 2008, respectively. From 2015, he has been with Samsung Medical Center, Seoul, South Korea, as a Research Staff Member. His current research focuses on application of implantable medical applications into the large animal experiment.

**Seunghun Lee** received the M.D. and M.S. degrees from Sungkyunkwan University, School of Medicine, Seoul, South Korea, in 2006 and 2012, respectively. Since 2018, he has been the Ph.D. candidate in functional neurosurgery. He completed his residency and clinical fellowship in neurosurgery with Samsung Medical Center, and currently. he is an Assistant Professor with the Neurosurgery Department of Samsung Medical Center. His current research interests include functional neurosurgery, especially epilepsy, and neurovascular compression syndrome.

**Joonseong Kang** received the B.S. degree in electrical engineering and M.S. degree in electrical and computer engineering from Seoul National University, Seoul, South Korea, in 2007 and 2009, respectively. He is currently working toward the Ph.D. degree with Seoul National University, as a Member of the Samsung Fellowship Program. Since 2009, he has been with Samsung Electronics Co., Ltd., Suwon, South Korea. His current research interests include the research and development of ultra-small and low power systems for bio-electronics.

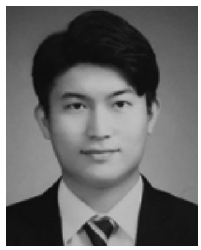

**Wonok Kang** received the B.S. degree in school of electronics engineering from Kyungpook National University, South Korea, in 2017. He is currently working toward the Ph.D. degree with Innovative Medical Solution Lab., the Pohang University of Science and Technology, Pohang, South Korea. His main research interests include neurostimulation, implantable medical device, and embedded system design.

**Sehyeon Kim** received the B.S. degree in electronic engineering from Soongsil University, Seoul, South Korea, in 2018. She is currently working toward the Ph.D. degree (M.S.–Ph.D. joint program) in creative IT engineering with the Pohang University of Science and Technology, Pohang, South Korea. Her current research interests include brain-computer interface for rehabilitation medicine and deep neural networks.

**Sung-Min Park** received the B.S. and Ph.D. degrees in electrical and computer engineering from Purdue University, West Lafayette, Indiana, U.S., in 2001 and 2006, respectively. Since 2016, he has been a Professor of the Department of Creative IT Engineering with the Pohang University of Science and Technology (POSTECH, Pohang, South Korea). From 2006 to 2014, he was with Medtronic (Minneapolis, Minnesota, U.S.) as R&D Manager, leading the award-wining effort in developing the world first MRI conditional pacemaker. From 2014 to 2016, he was with Samsung (Suwon, South Korea) as Director, spearheading healthcare centric mobile device and mobile health service platform development projects.

**Duk L. Na** is currently the Director of the Samsung Alzheimer's Research Center, Samsung Medical Center. He is also a Professor with the School of Medicine and Department of Health Sciences and Technology, Sungkyunkwan University. He completed his internship, residency, and MD training with the Seoul National University School of Medicine. For his Postdoctoral Research Fellowship training, He worked under the direct mentorship of Dr. Kenneth M. Heilman with the University of Florida (Gainesville, Florida). He is also the Principal Investigator of the Cognitive Neuroscience and Dementia Laboratory. He has authored or coauthored more than 250 articles on dementia and cognitive neuroscience in peer-reviewed, international journals. His research interests include developing a dementia prevention program based on cognitive training, early diagnosis of dementia by utilizing clinical biomarkers and virtual reality, inventing a device to repeatedly administer stem cells into the brain parenchyma, generation of AD specialized next generation MSCs, and AD disease modeling using patient-derived iPSCs. His honors include the Yoon Kwang-Yull Medical Prize (Korean Academy of Medical Sciences) and the Bayer Prize in Clinical Medicine (Korean Academy of Medical Sciences).

**Young-Min Shon** received the M.S. and Ph.D. degrees in medicine and neurology from Seoul National University, Sungkyunkwan University School of Medicine, in 1993 and 2006, respectively. Since 2016, he has beena Professor of the Department of Neurology with Samsung Medical Center (Seoul, ROK) . From 2002 to 2016, he worked with the Catholic University of Korea (Seoul, ROK) as a professor, leading the 1$^{st}$ trial and the settlement of deep brain stimulation for epilepsy in South Korea. His current research interests include neuromodulation & minimally invasive surgical therapy for intractable epilepsy and translational animal research for application of novel neuro-devices.

**Sang Joon Kim** (Member, IEEE) received the bachelor's degree in electrical engineering from Seoul National University, Seoul, South Korea, in 2001, and the master's degree in applied mathematics and the Ph.D. in engineering science from the School of Engineering and Applied Sciences, Harvard University, Cambridge, MA, in 2007 and 2009, respectively. Since 2009, he has been with the Samsung Advanced Institute of Technologies as a Research Staff Member. His current research interests include ultra-low power system design for medical, healthcare applications.